

Three-Dimensional Viscous Shock Layer Computation Using Axisymmetric Analogy Along the Streamlines

S. Noori, S.M.H. Karimian and S. Ghasemloo

Amirkabir University of Technology, Tehran, Iran, 15875-4413

Center of Excellence in Computational Aerospace Engineering

Abstract

An approximate method is developed to calculate three-dimensional viscous hypersonic equations, using axisymmetric analog. Three-dimensional viscous shock layer equations are reduced to an axisymmetric form by implementation of axisymmetric analogy along the streamlines. Maslen equation is still used instead of the normal momentum equation. Governing equations are solved in a streamline curvilinear coordinate system. In this case the method can predict convective heat flux in the leeward region where other similar methods are not applicable. Implementation of the axisymmetric analog results in a dramatic reduction of the CPU time of calculation, in comparison to the 3DVSL methods. The results are compared very well with the experimental and numerical data. Since this method is fast and accurate, it is an excellent tool for parametric study and preliminary design of hypersonic vehicles.

1. Introduction

Aerodynamic heating is an important issue in hypersonic flights. Therefore, accurate prediction of aerodynamic heating over the surface of the space vehicle would be very important. This can be done by the solution of Navier-Stocks equations [1,2] or the simplified form of these equations, such as VSL equations [3-6]. The VSL equations need less CPU time in comparison to the solution of full Navier-Stocks equations [7]. The VSL equations are obtained from the full Navier-Stocks equation by keeping terms up to second order in the inverse square root of Reynolds number [8]. These equations apply to both subsonic and supersonic regions. Since the exact solution of these equations require large computer storage and CPU time, they are not appropriate for preliminary design, where many trajectory points must be analyzed. Therefore many scientists searched for approximate methods.

An approximate axisymmetric method was developed by Grantz et al. [9]. In addition to using Maslen's [10] second-order pressure equation, he incorporated viscous terms into the streamwise momentum and energy equations, to obtain a simple method which can calculate both the subsonic and supersonic regions of the shock layer. His method does not require a starting solution for the shock shape. The shortcomings of the method, however, are the high number of iterations required for shock shape convergence, and its inconsistent solution near the stagnation line. In addition to this solution oscillations are seen in the shock layer due to the node distribution across this layer [11].

Another approximate axisymmetric method was developed by Cheatwood and DeJarnette [11]. Their method resolved the disadvantages of Grantz's method. The full VSL equations was solved in a shock coordinate system. Maslen's second-order pressure expression was replaced for the normal momentum equation and continuity equation was solved to find the normal component of velocity. In this method, shock shape is determined as a part of the solution in subsonic and supersonic regions.

Malekzadeh et al. [12] extended the method of Cheatwood and DeJarnette to cover three dimensional flow. In this method shock shape is determined using Riley and DeJarnette algorithm [13]. As reported in Ref. 12, this method is 3 to 5 times faster than the original 3DVSL methods [12], however it is capable of determining flow properties and

aerodynamic heating only in the windward region. To cover the calculation of aerodynamic heating in the leeward region using a fast method, the present work is developed. In this work, 3DVSL equations are reduced to an axisymmetric form using axisymmetric analog [14], which can be solved along the streamlines on the surface of the body. In fact, the laminar and turbulent 3DVSL equations are written in the streamline curvilinear coordinate system. The idea of using axisymmetric analog has caused a dramatic reduction of CPU time.

2. Governing Equations

Three-dimensional viscous shock layer equations are derived from the steady state Navier-Stokes equations. In this paper, the 3DVSL equations are written in a streamline curvilinear coordinate system of $\bar{\xi}, \bar{\beta}, \bar{n}$; see Figure 1. The coordinates $\bar{\xi}, \bar{\beta}$ represent a point on the surface of the body, and \bar{n} represent the distance normal to the body. Unit vectors $e_{\bar{\xi}}$ and $e_{\bar{\beta}}$, which are tangent to the body surface, are chosen such that $e_{\bar{\xi}}$ is in the direction of streamline and $e_{\bar{\beta}}$ is perpendicular to $e_{\bar{\xi}}$ and $e_{\bar{n}}$.

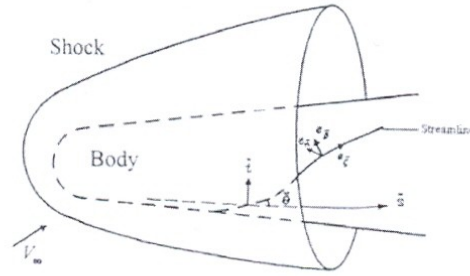


Figure 1: Streamline curvilinear coordinate system

The orientations of streamlines are required since the equations should be written along the streamlines. The method for the calculation of streamline orientation is presented in the Ref. [15]. To simplify the solution method, the governing equations are transformed from the $(\bar{\xi}, \bar{\beta}, \bar{n})$ system to a new computational coordinate system of $(\tilde{\xi}, \tilde{\beta}, \eta_n)$, where $\tilde{\xi} = \bar{\xi}$,

$$\tilde{\beta} = \bar{\beta}, \quad \eta_n = 1 + \frac{\bar{n}}{n_b}$$

In this transformed system, the governing equations of momentum are cased in the form of

$$A_0 \frac{\partial^2 W}{\partial \eta_n^2} + A_1 \frac{\partial W}{\partial \eta_n} + A_2 W + A_3 + A_4 \frac{\partial W}{\partial \tilde{\xi}} + A_5 \frac{\partial W}{\partial \tilde{\beta}} = 0$$

Where W represents the dependent variables u , w and h for $\bar{\xi}$ momentum, $\bar{\beta}$ momentum and energy equations, respectively. The nonlinear coefficients A_0, A_1, A_2, A_3, A_4 and A_5 are given in appendix .

The continuity equation is written in the form of

$$M \frac{\partial}{\partial \tilde{\xi}} (\rho u \bar{h}_3) + (MD + NF) \frac{\partial}{\partial \eta_n} (\rho u \bar{h}_3) + N \frac{\partial}{\partial \tilde{\beta}} (\rho u \bar{h}_3) - A \frac{\partial}{\partial \eta_n} (\rho v \bar{h}_1 \bar{h}_3) + T \frac{\partial}{\partial \tilde{\xi}} (\rho w \bar{h}_1) + (TD + KF) \frac{\partial}{\partial \eta_n} (\rho w \bar{h}_1) + K \frac{\partial}{\partial \tilde{\beta}} (\rho w \bar{h}_1) = 0$$

Where

$$A = \frac{1}{n_b}, \quad \bar{h}_1 = h_{\bar{\xi}}(1 + \bar{n}k_{\bar{\xi}}), \quad \bar{h}_3 = h_{\bar{\beta}}(1 + \bar{n}k_{\bar{\beta}})$$

And the streamline curvatures are defined as

$$k_{\bar{\xi}} = -\frac{1}{h_{\bar{\xi}}} \frac{\partial \bar{\Gamma}}{\partial \bar{\xi}}, \quad k_{\bar{\beta}} = -\frac{\cos \bar{\Gamma}}{h_{\bar{\beta}}} \frac{\partial \bar{\Gamma}}{\partial \bar{\beta}}$$

The values of M, N, T and K are functions of streamline curvatures, the distance between the body and shock, body angles, and finally shock angles.

3. Axisymmetric Analog

The Three Dimensional Boundary Layer analysis is simplified when using the axisymmetric analog. This is done in the most of engineering aerothermal calculations since it increasing the rate of convergence and therefore decreases the CPU time [14]. Since viscous shock layer equations are similar to the boundary layer equations, we can use the axisymmetric analog for 3DVSL equations as well. In this paper axisymmetric analog is implemented in the streamline curvilinear coordinate system. For this purpose, the crossflow velocity component (w) is neglected in the 3DVSL equations. Besides its advantages in reducing CPU time, axisymmetric analog provides streamline orientation in the leeward region, and therefore the flow field can be solved in this region as well.

4. Boundary Conditions

Appropriate boundary conditions along the shock wave and the body surface must be specified. The conditions behind the shock are obtained from the Rankin – Hugoniot relations. The no-slip Conditions of $u = v = w = 0$ are applied on the wall, and the fixed temperature of wall are applied for the energy equation.

5. Solution Scheme

In the present method the governing equations are solved for a determined shock shape. This shock shape is calculated from the approximate method of Riley and DeJarnette[13]. Since their method is an inverse one, the shock shape is determined from an iterative process. Having known the shock shape, the axisymmetric viscous shock layer equations in the streamline coordinate system are solved along the lines between normal to the shock, within the shock layer. They are solved, first along the stagnation line and then along the similar lines downstream and around the body (figure 2). At each point of these normal lines the equations are solved in the following order for both laminar and turbulent flow.

1. Pressure is calculated from the Maslen's relation.
2. Tangential velocity and enthalpy are determined from the solution of streamwise momentum and energy equations.
3. Density is calculated from the equation of state.
4. Normal velocity is calculated from the solution of continuity equation

For turbulent flow, the e

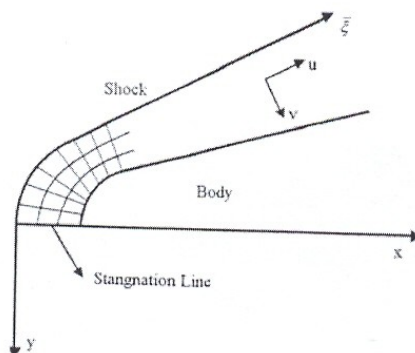


Figure 2: Computational grid between shock and body

6. Results

Surface heating rate distributions are calculated for laminar and turbulent perfect gas flows over a 15 deg. half angle blunted cone at two angles of attack to validate the present method. The accuracy of this method is demonstrated by comparison of the present results with the experiment [16], and other numerical predictions. The variables are nondimensionalized as: lengths by R_{nose} , pressure by $\rho_{\infty} v_{\infty}^2$, enthalpy by v_{∞}^2 , and heating rate by $\rho_{\infty} v_{\infty}^3$. The freestream Conditions are $\rho_{\infty} = 0.00973 \text{ kg/m}^3$, $T_{\infty} = 47.3^{\circ} \text{ K}$ and $M_{\infty} = 10.6$. The wall temperature is fixed to $T_w = 300^{\circ} \text{ K}$. The solution is marched in the ξ direction with the step size of $0.03R_{nose}$. In the η_n direction, however, the spacing of nodes is variable. In fact more nodes are located near the wall. Our experience shows that 51 nodes in this direction is optimum interms of accuracy and less CPU time.

1.6 Laminar Flow Comparison

Figures 3 and 4 show the heating rate in windward plane at 5 and 10 degrees of angle of attack for two spherical nose radii of $R_{nose} = 0.00952 \text{ m}$ and $R_{nose} = 0.0279 \text{ m}$, respectively. Excellent agreement is seen between the results of present method with the experimental data.

For the first time the approximate solution of VSL equations are used to predict the heat heating rates in the leeward region by the present method. For the R_{nose} of 0.0279 m at 5 and 10 degrees angle of attack, the heating rates on the leeward plane are present in Figure 5. Since the shock layer in the leeward region is thick, the Maslen's assumption is violated. As a result small differences between the results of the present method and the experimental data are

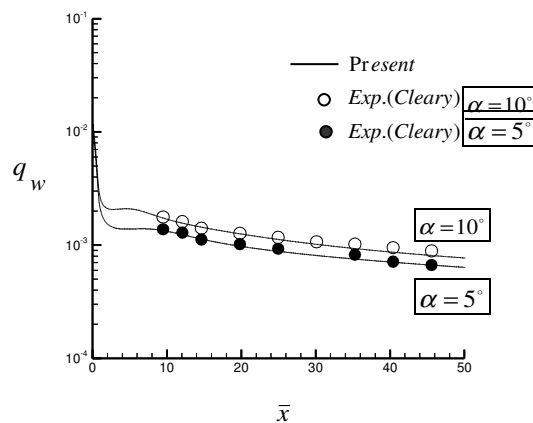


Figure 3: Heat transfer comparison in windward plane, $R_{nose} = 0.00952m$

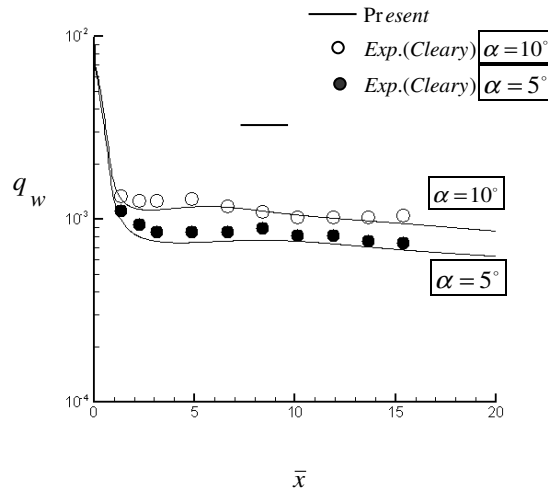


Figure 4: Heat transfer comparison in windward plane, $R_{nose} = 0.00952m$

observed. At axial location of 10.13 R_{nose} of a 15 degree sphere cone with $R_{nose} = 0.0279m$, the heating rates in the circumferential direction are presented for two angles of attack in Figure 6. For $R_{nose} = 0.00952m$ the heating rates are given at two axial locations in Figure 7. As is seen in these figures, present results agree very well with the experimental data in both windward and leeward regions.

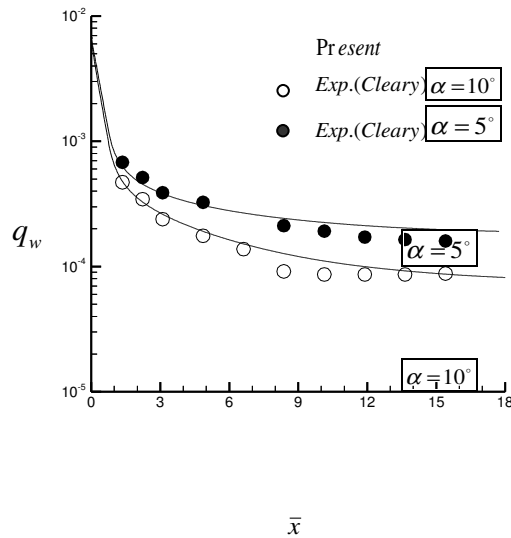
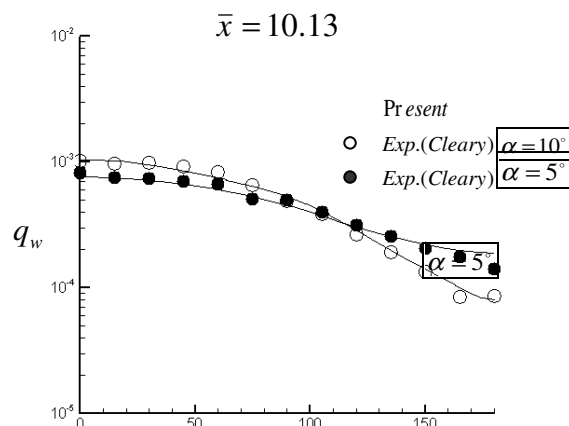


Figure 5: Heat transfer comparison in leeward plane, $R_{nose} = 0.0279m$



$\alpha = 10^\circ$

$\bar{\phi}$ (deg)

Figure 6: Circumferential Heat transfer comparison, $R_{nose} = 0.0279m$

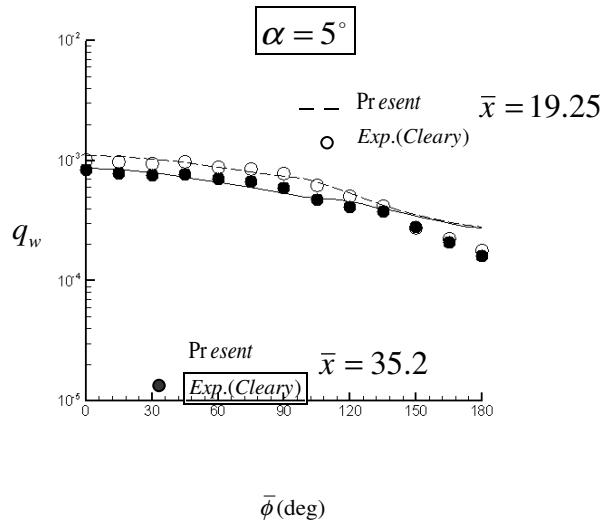
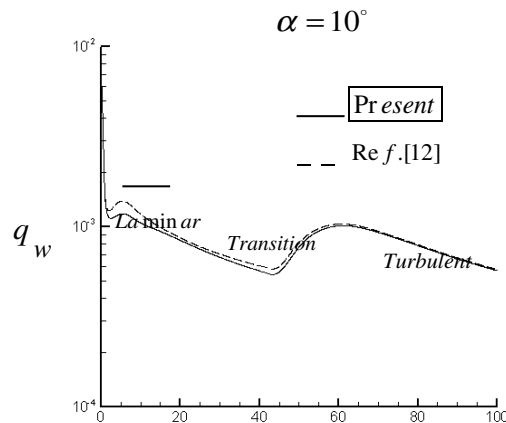


Figure 7: Circumferential Heat transfer comparison at two axial location, $R_{nose} = 0.00952m$

1.6 Turbulent Flow Comparison

The comparison of turbulent heating rate predictions and the other numerical data [12] are shown for a 15 degree sphere cone with two R_{nose} of 0.00952m and 0.0279m in figures 8 and 9. The transition of laminar flow to turbulent flow occurs at $\bar{x} = 40$ and $\bar{x} = 30$ in figures 8 and 9, respectively. The predicted heating rates of the present method and those of the method of Ref. 12 are in very good agreement with each other. The advantage of the present method to the method of Ref. 12 is a 35 percent reduction in the CPU time. In preliminary design, this reduction is very important.



\bar{x}

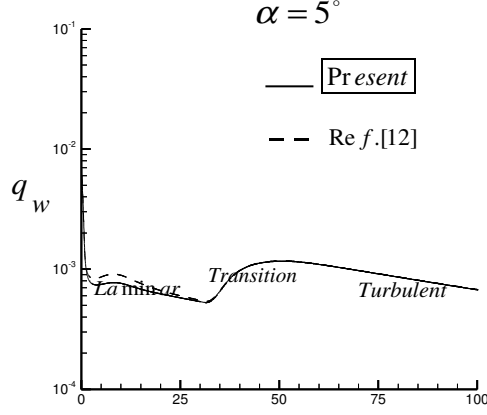
 Figure 8: Heat transfer comparison in windward plane, $R_{nose} = 0.0279m$

 \bar{x}

 Figure 9: Heat transfer comparison in windward plane, $R_{nose} = 0.00952m$

Appendix

Momentum and energy equations may be written in the form of

$$A_0 \frac{\partial^2 W}{\partial \eta_n^2} + A_1 \frac{\partial W}{\partial \eta_n} + A_2 W + A_3 + A_4 \frac{\partial W}{\partial \xi} + A_5 \frac{\partial W}{\partial \beta} = 0$$

Where W represents the dependent variables u, w and h for ξ momentum, β momentum and energy equations, respectively. The nonlinear coefficients A_0, A_1, A_2, A_3, A_4 and A_5 are

ξ Momentum

$$A_0 = -\frac{\varepsilon^2}{\rho} \mu A^2 (1 + \varepsilon^+)$$

$$A_1 = -\nu A - \frac{\varepsilon^2}{\rho} A^2 \frac{\partial \mu}{\partial \eta_n} (1 + \varepsilon^+) - \frac{\varepsilon^2}{\rho} \mu A^2 \frac{1}{h_1} \frac{\partial \bar{h}_1}{\partial \eta_n} + \frac{\varepsilon^2}{\rho} \mu A^2 \left(\frac{2}{h_1} \frac{\partial \bar{h}_1}{\partial \eta_n} + \frac{1}{h_3} \frac{\partial \bar{h}_3}{\partial \eta_n} \right) (1 + \varepsilon^+) + (MD + NF) \frac{u}{h_1} +$$

$$(TD + KF) \frac{w}{h_3} - \frac{\varepsilon^2}{\rho} \mu A^2 \frac{\partial \varepsilon^+}{\partial \eta_n}$$

$$A_2 = -\nu A \frac{1}{h_1} \frac{\partial \bar{h}_1}{\partial \eta_n} + \frac{w}{h_1 h_3} \left[T \frac{\partial \bar{h}_1}{\partial \xi} + (TD + KF) \frac{\partial \bar{h}_1}{\partial \eta_n} + K \frac{\partial \bar{h}_1}{\partial \beta} \right] + \frac{\varepsilon^2}{\rho} A^2 \frac{\partial \mu}{\partial \eta_n} \frac{1}{h_1} \frac{\partial \bar{h}_1}{\partial \eta_n} + \frac{\varepsilon^2}{\rho} \mu A^2 \left(\frac{1}{h_1} \frac{\partial \bar{h}_1}{\partial \eta_n} \right) \left(\frac{2}{h_1} \frac{\partial \bar{h}_1}{\partial \eta_n} + \frac{1}{h_3} \frac{\partial \bar{h}_3}{\partial \eta_n} \right)$$

$$A_3 = -\frac{w^2}{h_1 h_3} \left[M \frac{\partial \bar{h}_3}{\partial \xi} + (MD + KF) \frac{\partial \bar{h}_3}{\partial \eta_n} + N \frac{\partial \bar{h}_3}{\partial \beta} \right] + \frac{1}{\rho h_1} \left[M \frac{\partial P}{\partial \xi} + (MD + KF) \frac{\partial P}{\partial \eta_n} + N \frac{\partial P}{\partial \beta} \right]$$

$$A_4 = \frac{u}{h_1} M + \frac{w}{h_3} T, A_5 = \frac{u}{h_1} N + \frac{w}{h_3} K$$

$\bar{\beta}$ Momentum

$$A_0 = -\frac{\varepsilon^2}{\rho} \mu A^2$$

$$A_1 = -vA - \frac{\varepsilon^2}{\rho} A^2 \frac{\partial \mu}{\partial \eta_n} - \frac{\varepsilon^2}{\rho} \mu A^2 \left(\frac{1}{\bar{h}_1} \frac{\partial \bar{h}_1}{\partial \eta_n} + \frac{1}{\bar{h}_3} \frac{\partial \bar{h}_3}{\partial \eta_n} \right) + (MD + NF) \frac{u}{\bar{h}_1} + (GD + KF) \frac{w}{\bar{h}_3}$$

$$A_2 = -vA \frac{1}{\bar{h}_3} \frac{\partial \bar{h}_3}{\partial \eta_n} + \frac{u}{\bar{h}_1 \bar{h}_3} \left[M \frac{\partial \bar{h}_3}{\partial \xi} + (MD + KF) \frac{\partial \bar{h}_3}{\partial \eta_n} + \right.$$

$$\left. N \frac{\partial \bar{h}_3}{\partial \beta} \right] + \frac{\varepsilon^2}{\rho} A^2 \frac{\partial \mu}{\partial \eta_n} \frac{1}{\bar{h}_3} \frac{\partial \bar{h}_3}{\partial \eta_n} + \frac{\varepsilon^2}{\rho} \mu A^2 \frac{1}{\bar{h}_3} \left(\frac{\partial \bar{h}_3}{\partial \eta_n} \right)^2 +$$

$$\frac{\varepsilon^2}{\rho} \mu A^2 \frac{1}{\bar{h}_1 \bar{h}_3} \frac{\partial \bar{h}_1}{\partial \eta_n} \frac{\partial \bar{h}_3}{\partial \eta_n}$$

$$A_3 = -\frac{u}{\bar{h}_1 \bar{h}_3} \left[T \frac{\partial \bar{h}_1}{\partial \xi} + (TD + KF) \frac{\partial \bar{h}_1}{\partial \eta_n} + K \frac{\partial \bar{h}_1}{\partial \beta} \right] +$$

$$\frac{1}{\rho \bar{h}_3} \left[T \frac{\partial P}{\partial \xi} + (TD + KF) \frac{\partial P}{\partial \eta_n} + K \frac{\partial P}{\partial \beta} \right]$$

$$A_4 = \frac{u}{\bar{h}_1} M + \frac{w}{\bar{h}_3} T, A_5 = \frac{u}{\bar{h}_1} N + \frac{w}{\bar{h}_3} K$$

Energy

$$A_0 = -\frac{\varepsilon^2}{\rho} \frac{\mu}{\text{Pr}} A^2 (1 + \varepsilon^+ \frac{\text{Pr}}{\text{Pr}_t})$$

$$A_1 = -vA - \frac{\varepsilon^2}{\rho} \frac{A^2}{\text{Pr}} \frac{\partial \mu}{\partial \eta_n} (1 + \varepsilon^+ \frac{\text{Pr}}{\text{Pr}_t}) - \frac{\varepsilon^2}{\rho} \frac{\mu}{\text{Pr}_t} A^2 \frac{\partial \varepsilon^+}{\partial \eta_n} - \frac{\varepsilon^2}{\rho} \frac{\mu}{\text{Pr}} \left(\frac{1}{\bar{h}_1} \frac{\partial \bar{h}_1}{\partial \eta_n} + \frac{1}{\bar{h}_3} \frac{\partial \bar{h}_3}{\partial \eta_n} \right) (1 + \varepsilon^+ \frac{\text{Pr}}{\text{Pr}_t}) + (MD + NF) \frac{u}{\bar{h}_1} +$$

$$(TD + KF) \frac{w}{\bar{h}_3}$$

$$A_2 = 0$$

$$A_3 = \frac{vA}{\rho} \frac{\partial P}{\partial \eta_n} - \frac{u}{\rho \bar{h}_1} \left[M \frac{\partial P}{\partial \xi} + (MD + KF) \frac{\partial P}{\partial \eta_n} + N \frac{\partial P}{\partial \beta} \right] - \frac{w}{\rho \bar{h}_3} \left[T \frac{\partial P}{\partial \xi} + (TD + KF) \frac{\partial P}{\partial \eta_n} + K \frac{\partial P}{\partial \beta} \right] - \frac{\varepsilon^2}{\rho} \mu \left(\frac{u}{\bar{h}_1} \frac{\partial \bar{h}_1}{\partial \eta_n} A \right)^2 -$$

$$\frac{\varepsilon^2}{\rho} \mu (1 + \varepsilon^+) \left[\left(A \frac{\partial u}{\partial \eta_n} \right)^2 - 2A^2 \frac{u}{\bar{h}_1} \frac{\partial \bar{h}_1}{\partial \eta_n} \frac{\partial u}{\partial \eta_n} \right]$$

$$A_4 = \frac{u}{\bar{h}_1} M + \frac{w}{\bar{h}_3} T, A_5 = \frac{u}{\bar{h}_1} N + \frac{w}{\bar{h}_3} K$$

References

- [1] Gnoffo P. A. An upwind-Biased Point Implicit Relaxation Algorithm for Viscous, Compressible Perfect-Gas Flows. NASA TP 2953, June 1990.
- [2] Miyaji K. and Fujii K. Numerical Analysis of Three-Dimensional Shock/Shock Interactions and the Aerodynamic Heating. AIAA- 99-0144, 1999.

- [3] Davis R. T. Numerical Solution of the Hypersonic Viscous Shock Layer Equations.” *AIAA Journal*, Vol. 8, No. 5, May1970, PP. 843-851.
- [4] Maslov A. A., Mironov S. G., Poplavaskaya T. V., Shilyuk A. N., Vetlutsky V. N. Viscous Shock Layer on a Plate in Hypersonic Flow. *Eur. J. Mech. B/Fluids*, Vol. 18, No. 2, 1999.
- [5] Gupta R. N., Zoby E.V. , Nayani S. N., Lee K. P. High – Order Viscous Shock-Layer Solutions for High-Altitude Flows. *Journal of spacecraft and Rockets*, Vol. 31, No.5, 1994, pp. 751-758.
- [6] Gupta R. N., Lee K.P., Zoby E.V., Moss J. N., and Thompson R. A. Hypersonic Viscous Shock-Layer Solutions over Long Slender Bodies-Part I: High Reynolds Number Flows. *Journal of spacecraft*, Vol. 27, No. 2, March-April 1990.
- [7] Srivastava B. N., Werle M.J., Davis R.T. Viscous Shock-Layer Solutions for Hypersonic Sphere-Cones. AIAA paper 77-693, June 1977.
- [8] Murray A. L., Lewis C. H. Hypersonic Three-Dimensional Viscous Shock Layer Flows Over Blunt Bodies. *AIAA Journal*, Vol. 16, No.12, 1978, pp. 1279-1286.
- [9] Grantz A. C., DeJarnette F. R., Thompson R. A. Approximate Viscous-Shock Layer Method for Hypersonic Flows over Blunt-Nosed Bodies. *Journal of Spacecraft and Rockets*, Vol. 27, No. 6, 1990, pp. 597-605.
- [10]Maslen S. H Inviscid Hypersonic Flow Past Smooth Symmetric Bodies. *AIAA Journal*, Vol. 2, July 1964, pp. 1055-1061.
- [11]Cheatwood F. M., DeJamentte F. R. Approximate Viscous Shock-Layer Technique for Calculating Hypersonic Flows About Blunt. Nosed Bodies. *Journal of Spacecraft and Rockets*, Vol. 31, No. 4, 1994, pp. 621-628.
- [12]Malekzadeh Dirin M., Marefat M., Karimian S. M H. Approximate Three-Dimensional Viscous Shock-Layer Method for Hypersonic Flow over Blunt-Nosed Bodies. AIAA Paper 03-154, 2003.
- [13]Riley C. J., DeJarnette F. R. Engineering Aerodynamic Heating Method for Hypersonic Flow. *Journal of Spacecraft and Rockets*, Vol. 29, No.3, May-June 1992.
- [14]Cook J. C. An Axially Symmetiric Analogue for General Three-Dimensional Boundary Layer. British A.R.C., R & M, No. 3200, 1961.
- [15]Maerefat, M., Karimian, S.M.H., Malekzadeh Dirin, M. An Engineering Inviscid-Boundary Layer Method for Calculation of Aerodynamic Heating in the Leeward Region. *Iranian Journal of Science & Technology, Transaction B, Engineering*, Vol. 31, No. B1, pp 13-30, 2007.
- [16]Cleary J. W. Effects of Angle of Attack and Bluntness on Laminar Heating Rate Distribution on a 15 Degree Cone at a Mach Number of 10.6. NASA TN5450,October 1969.



This page has been purposely left blank